THE AMERICAN SOCIETY OF MECHANICAL ENGINEERS
345 E. 47 St., New York, N.Y. 10017

92-GT-199

Interactions Between Embedded Vortices and Injectant From Film Cooling Holes with Compound Angle Orientations in a Turbulent Boundary Layer

P. M. LIGRANI* and S. W. MITCHELL+

Department of Mechanical Engineering, Naval Postgraduate School
Monterey, California 93943-5000

ABSTRACT

Experimental results are presented which describe the effects of embedded, longitudinal vortices on heat transfer and film injectant downstream of two staggered rows of film cooling holes with compound angle orientations. Holes are oriented so that their angles with respect to the test surface are 30 degrees in a spanwise/normal plane projection, and 35 degrees in a streamwise/normal plane projection. A blowing ratio of 0.5, non-dimensional injection temperature parameter θ of about 1.5, and freestream velocity of 10 m/s are employed. Injection hole diameter is 0.945 cm to give a ratio of vortex core diameter to hole diameter of 1.6-1.67 just downstream of the injection holes (x/d=10.2). At the same location, vortex circulation magnitudes range from 0.15 m^2/s to 0.18 m^2/s. By changing the sign of the angle of attack of the half-delta wings used to generate the vortices, vortices are produced which rotate either clockwise or counter-clockwise when viewed looking downstream in spanwise/normal planes.

The most important conclusion is that local heat transfer and injectant distributions are strongly affected by the longitudinal embedded vortices, including their directions of rotation and their spanwise positions with respect to film injection holes. Differences resulting from vortex rotation are due to secondary flow vectors, especially beneath vortex cores, which are in different directions with respect to the spanwise velocity components of injectant after it exits the holes. When secondary flow vectors near the wall are in the same direction as the spanwise components of the injectant velocity (clockwise rotating vortices R0-R4), the film injectant is more readily swept beneath vortex cores and into vortex upwash regions than for the opposite situation in which near-wall secondary flow vectors are opposite to the spanwise components of the injectant velocity (counter-clockwise rotating vortices L0-L4). Consequently, higher St/Sto are present over larger portions of the test surface with vortices R0-R4 than with vortices L0-L4. These disruptions to the injectant and heat transfer from the vortices are different from the disruptions which result when similar vortices interact with injectant from holes with simple angle orientations. Surveys of streamwise mean velocity, secondary flow vectors, total pressure, and streamwise mean vorticity are also presented which further substantiate these findings.

* Associate Professor, +Graduate Student

NOMENCLATURE

A	vortex generator delta wing angle of attack
c	average vortex core radius
C_p	specific heat
d	injection hole diameter
m	blowing ratio, $\rho_c U_c / \rho_\infty U_\infty$
S	non-dimensional circulation, $\Gamma / U_c\, d$
S1	non-dimensional circulation, $\Gamma / U_c\, 2\, c$
St	Stanton number with vortex and film injection
Sto	baseline Stanton number, no vortex, no film injection
Stf	Stanton number with film injection and no vortex
T	static temperature
U	mean velocity
X,x	streamwise distance
Y	distance normal to the surface
Z	spanwise distance from test surface centerline
ξ	unheated starting length
ρ	density
θ	non-dimensional injection temperature, $(T_{r,c} - T_{r,\infty})/(T_w - T_{r,\infty})$
Γ	circulation of streamwise vorticity

Subscripts

c	injectant at exits of injection holes
r	recovery condition
w	wall
y	normal component
z	spanwise component
∞	freestream

INTRODUCTION

Accounting for the presence of embedded longitudinal vortices is important for the design of cooling schemes for turbine blades and turbine endwalls. This is because embedded vortices are abundant in the passages between turbine blades. In addition, their presence results in significant perturbations to distributions of film coolant along with the accompanying thermal protection. Of importance are the magnitudes of perturbations to wall heat transfer and injectant distributions resulting from the interactions between the vortices and the film coolant, as illustrated by a number of recent studies. These include investigations of the interactions of embedded vortices

Presented at the International Gas Turbine and Aeroengine Congress and Exposition
Cologne, Germany June 1-4, 1992
This paper has been accepted for publication in the Transactions of the ASME
Discussion of it will be accepted at ASME Headquarters until September 30, 1992

with film injection from slots (Blair, 1974), with film injection from rows of holes (Goldstein and Chen, 1985, 1987; Ligrani et al.,1989a, 1991), as well as with film injectant from a single hole (Ligrani and Williams, 1990). According to Ligrani et al. (1991), the complicated nature of these physical situations results because of the dependence of local heat transfer and injection distributions on vortex strength, vortex size, and vortex location relative to a vast array of film cooling injection rates, hole sizes, geometries and configurations.

Experimental studies of the interactions of embedded vortices and film cooling are scarce. Of earlier studies, Blair (1974) reports heat transfer distributions measured on an endwall film-cooled using a slot inclined at a 30 degree angle. The large vortex located in the corner between the endwall and the suction surface of their cascade was believed to cause significant variations of measured heat transfer and film cooling effectiveness. Nicolas and LeMeur (1974), Folayan and Whitelaw (1976), and Mayle et al. (1977) all focus on the effects of wall curvature, as well as the resulting arrays of vortex pairs, on the performance of film cooling over turbine blades. Goldstein and Chen (1985, 1987) describe results from a study on the influence of flows originating near the endwall on blade film cooling from one and two rows of holes. A triangular region is described which exists on the convex side of the blade where coolant was swept away from the surface by the passage vortex.

Ligrani et al. (1989a) describe the influences of embedded longitudinal vortices on film cooling from a single row of film cooling holes in a turbulent boundary layer. In that study, each hole is inclined at an angle of 30 degrees with respect to the test surface, and spaced 3-hole diameters from neighboring holes. Surface heat transfer distributions, mean velocities, and mean temperatures show that film coolant is greatly disturbed and local Stanton numbers are altered significantly by the secondary flows within vortices. To further clarify the interactions between vortices and wall jets, Ligrani and Williams (1990) examined the effects of an embedded vortex on injectant from a single film-cooling hole in a turbulent boundary layer. Attention is focussed on the effect of spanwise position of the vortices with respect to film injection holes. The main conclusion is that injection hole centerlines must be at least 2.9-3.4 vortex core diameters away from the vortex center in the lateral direction to avoid significant alterations to wall heat transfer and distributions of film coolant. Ligrani et al. (1991) then considered the influences of vortex strength on heat transfer and injectant distributions downstream of a single row of holes having the same geometry employed by Ligrani et al. (1989a). In Ligrani et al. (1991), a variety of vortex strengths are considered, with circulations as large as 0.150 m^2/s. One of the most important conclusions from this study is that magnitudes of perturbations to injectant distributions are dependent upon the ratio of vortex circulation to injection velocity times hole diameter ($S = \Gamma/U_c\ d$), and the ratio of vortex circulation to injection velocity times vortex core diameter ($S1 = \Gamma/U_c\ 2c$).

Of existing studies which focus on interactions between the vortices and injectant from one or more holes, hole geometries in all cases are oriented with simple angles. Simple angle injection refers to situations in which the film is injected from holes inclined to the test surface such that injectant is issued from the holes at an angle with respect to the test surface when viewed in the streamwise/normal plane, but approximately in the direction of the mainstream flow when viewed in the streamwise/spanwise plane.

More recently, gas turbine components include film holes with compound angle orientations which are believed to produce injectant distributions over surfaces giving better protection and higher film effectivenesses than injectant from holes with simple angle orientations. Compound angle orientations are ones in which the film is injected with holes inclined to the test surface such that the injectant is issued with a spanwise velocity component relative to the mainstream flow (when viewed in the streamwise/spanwise plane). Consequently, interactions between vortices and film injection from holes with compound angle orientations are important because: (1) compound angle holes are now quite common on gas turbine components, and (2) the interactions are different from ones existing when simple angle holes are employed. To the best of the authors' knowledge, no data is available in the archival literature on heat transfer and boundary layer behavior downstream of film cooling holes with compound angle orientations when the injectant interacts with embedded longitudinal vortices. Thus, the purpose of the present study is to provide new physical understanding of such interactions.

The present study is therefore different from Ligrani, et al (1989a, 1991) and Ligrani and Williams (1989) because interactions between the vortices and injectant from film holes with compound angle configurations, instead of simple angle configurations, are considered. Heat transfer, mean velocity components, and injection distributions are measured downstream of two staggered rows of injection holes with compound angle geometry with a blowing ratio of 0.5. Both clockwise rotating vortices and counter-clockwise rotating vortices are employed, where vortex orientations are given as the vortices are viewed in spanwise/normal planes looking downstream. The direction of rotation of the vortices is important because rotation direction changes result in sign changes to the direction of secondary flow vectors near the wall beneath vortex cores. These are then opposed to or coincident with the spanwise velocity components of the injectant. Vortices are generated using half-delta wings placed on the wind tunnel test surface. The direction of vortex rotation is changed by altering the angle of delta wings with respect to the streamwise direction, and vortex spanwise positions with respect to the film injection holes are altered by changing the spanwise positions of the vortex generators.

EXPERIMENTAL APPARATUS AND PROCEDURES

Wind tunnel and coordinate system.

The wind tunnel is the same one used in the experiments of Ligrani et al. (1989a, 1991). The facility is open-circuit, subsonic, and located in the laboratories of the Department of Mechanical Engineering of the Naval Postgraduate School. A centrifugal blower is located at the upstream end, followed by a diffuser, a header containing a honeycomb and three screens, and then a 16 to1 contraction ratio nozzle. The nozzle leads to the test section which is a rectangular duct 3.05 m long and 0.61 m wide, with a topwall having adjustable height to permit changes in the streamwise pressure gradient.

A schematic showing the test section and coordinate system is presented in Fig. 1. The vortex generator base plate is shown to be located 0.48 m downstream of the boundary layer trip. The left edge of this base plate (looking downstream) is the base edge refered to in Table 1 as a location reference line. The downstream edge of the injection holes is then 0.584 m further downstream from this base plate. The surface used for heat transfer measurements is then located a short distance farther downstream. With this surface at elevated temperature, an unheated starting length of 1.077 m exists, and the direction of heat transfer is then from the wall to the gas. Thermocouple row locations along the test surface are also labelled in Fig. 1. In regard to the coordinate system, Z is the spanwise coordinate measured from the test section centerline, X is measured from the upstream edge of the boundary layer trip, and Y is measured normal to the test surface. x is measured from the downstream edge of the injection holes and generally presented as x/d.

Injection system.

The injection system is described by Ligrani, et al (1989a, 1991). Air for the injection system originates in a 1.5 horsepower DR513 Rotron Blower capable of producing 30 cfm at 2.5 psig. From the blower, air flows through a regulating valve, a Fisher and Porter rotometer, a diffuser, and finally into the injection heat exchanger and plenum chamber. The exchanger provides means to heat the injectant above ambient temperature. With this system and test plate heating, the non-dimensional injection temperature parameter θ was maintained at about 1.5 for all tests to maintain conditions similar to ones existing in gas turbine components. The plenum connects to thirteen plexigless tubes, each 8 cm long with a length/diameter ratio of 8.4. With no vortex present, boundary layer displacement thickness at the injection location is 0.28d.

Injection system performance was checked by measuring discharge coefficients which compared favorably with earlier measurements. Procedures to measure discharge coefficients and blowing ratios are described by Ligrani et al. (1989a).

Experimental approach.

In order to isolate the interactions between film injectant and the vortices embedded in turbulent boundary layers, measurements are made on a flat plate in a zero pressure gradient. Wind tunnel speed is 10 m/s, and temperature differences are maintained at levels less than 30 degrees Centigrade so that viscous dissipation is negligible and fluid properties are maintained approximately constant. With this approach, many of the other effects present in high-temperature engines are not present (curvature, high free-stream turbulence, variable properties, stator/blade wake interactions, shock waves, compressibility, rotation, etc.) since these may obscure and complicate the interaction of interest.

Detailed measurements are made in spanwise planes at different streamwise locations in order to elucidate the development and evolution of flow behavior. In order to match the experimental conditions found in many practical applications, the boundary layer, embedded vortices, and wall injection are all turbulent.

Mean velocity components.

Three mean velocity components were measured using a five-hole pressure probe with a conical tip manufactured by United Sensors Corporation. Celesco transducers and Carrier Demodulators are used to sense pressures when connected to probe output ports. Following Ligrani et al. (1989b), corrections were made to account for spatial resolution and downwash velocity effects. The same automated traverse used for injectant surveys was used to obtain surveys of secondary flow vectors, from which, mean streamwise vorticity contours were calculated. These devices, measurement procedures employed, as well as data acquisition equipment and procedures used are further detailed by Ligrani et al. (1989a, 1989c).

Stanton number measurements.

Details on measurement of local Stanton numbers are given by Ortiz(1987), Bishop(1990), and Ligrani et al. (1989a, 1991). An overview of these procedures is repeated here for completeness.

The heat transfer surface is designed to provide a constant heat flux over its area. The surface next to the airstream is stainless steel foil painted flat black. Immediately beneath this is a liner containing 126 thermocouples, which is just above an Electrofilm Corp. etched foil heater rated at 120 volts and 1500 watts. Located below the heater are several layers of insulating materials including Lexan sheets, foam insulation, styrofoam and balsa wood. Surface temperature levels and convective heat transfer rates are controlled by adjusting power into the heater using a Standard Electric Co. Variac, type 3000B. To determine the heat loss by conduction, an energy balance was performed. Radiation losses from the top of the test surface were analytically estimated. The thermal contact resistance between thermocouples and the foil top surface was estimated on the basis of outputs of the thermocouples and measurements from calibrated liquid crystals on the surface of the foil. This difference was then correlated as a function of heat flux through the foil. The convective heat flux q and surface temperature T_w are then used to determine Stanton numbers using $St=q/((T_w-T_{r,\infty}) \rho_\infty U_\infty Cp)$.

After the surface was completed, a variety of qualification tests were conducted to check its performance. These are described in detail by Ortiz (1987).

Mean temperature measurements.

Copper-constantan thermocouples were used to measure temperatures along the surface of the test plate, the freestream temperature, as well as temperature distributions which are correlated to injection distributions. For the distributions, a thermocouple was traversed over spanwise/normal planes (800 probe locations) using an automated two-dimensional traversing system which could be placed at different streamwise locations. Ligrani et al. (1989a, 1991) give additional details including procedures used for calibration.

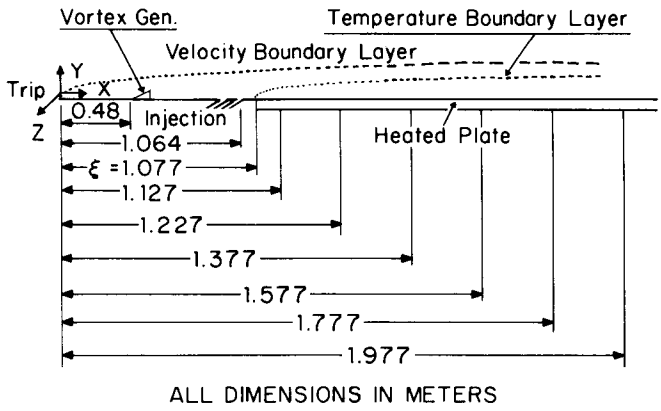

Figure 1. Schematic of wind tunnel test section.

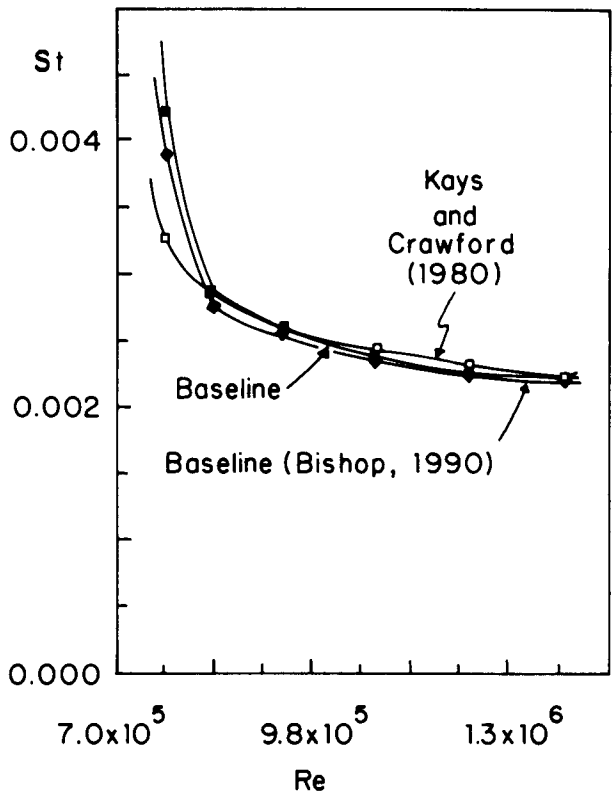

Figure 2. Baseline heat transfer data with no vortices and no film-cooling in the form of spanwise-averaged Stanton numbers as dependent upon Reynolds number.

Baseline data checks.

Baseline data with no film injection already exist for similar test conditions (Ligrani et al., 1989a). Figure 2 shows that repeated measurements of spanwise-averaged Stanton numbers show good agreement (maximum deviation is 5 percent) with the correlation from Kays and Crawford (1980) for turbulent heat transfer to a flat plate with unheated starting length and constant heat flux boundary condition. Also included on this figure are results from Bishop (1990), which also show good agreement with the correlation of Kays and Crawford (1980). Local and spanwise-averaged Stanton numbers with injection at a blowing ratio of 0.5 (and no vortex) also show agreement with earlier results (Ligrani et al., 1989a).

Vortex Label	Spanwise location of the vortex generator baseplate reference line, a (cm)	a/2s	Centerline injection hole location with respect to the vortices	Vortex center z spanwise locations at x/d=10.2
R0	0.0	0.00	Beneath downwash	-3.05 (-3.05*)
R1	1.8	0.24	Beneath downwash & core	-1.25
R2	3.6	0.49	Beneath upwash & core	0.55
R3	5.4	0.73	Beneath upwash	2.35
R4	7.2	0.98	Beneath side of upwash	4.15(4.06*)
L0	0.0	0.00	Beneath downwash	2.54(2.54*)
L1	-1.8	-0.24	Beneath downwash & core	0.74
L2	-3.6	-0.49	Beneath upwash & core	-1.06
L3	-5.4	-0.73	Beneath upwash	-2.86
L4	-7.2	-0.98	Beneath side of upwash	-4.66(-5.08*)

Table 1. Spanwise positions of the vortices and vortex generators. * Determined from vorticity survey measurements.

Further checks on measurement apparatus and procedures were made by measuring spatial variations of Stanton numbers along the test surface with different strength vortices (and no injection). These data are also consistent with other results in the literature (Ligrani et al., 1989a, 1991).

Experimental uncertainties.

Uncertainty analysis details are given by Ligrani et al. (1991). Uncertainty estimates are based upon 95 percent confidence levels, and determined following procedures described by Kline and McClintock (1953) and Moffat (1982). Typical nominal values of freestream recovery temperature and wall temperature are 18.0 and 40.0 degrees Centrigrade, with respective uncertainties of 0.13 and 0.21 degrees Centigrade. The freestream density, freestream velocity and specific heat uncertainties are 0.009 kg/m^3 (1.23 kg/m^3), 0.06 m/s (10.0m/s) and 1 J/kgK (1006 J/kgK), where typical nominal values are given in parentheses. For convective heat transfer, heat transfer coefficient, and heat transfer area, 10.5 W (270 W), 1.03 W/m^2 K (24.2 W/m^{2}K), and 0.0065 m^2 (0.558 m^2) are typical uncertainties. The uncertainties of St, St/Sto, m and x/d are 0.000086 (0.00196), 0.058 (1.05), 0.025 (0.50), and 0.36 (41.9).

In percentages, uncertainties of these quantities are as follows: freestream recovery temperature: 0.7, wall temperature: 0.5, freestream density: 0.7, freestream velocity: 0.6, specific heat: 0.1, convective heat transfer: 3.9, heat transfer coefficient: 4.3, heat transfer area: 1.2, St: 4.4, St/Sto: 5.5, m: 5.0, and x/d: 0.9.

INJECTION HOLE ARRANGEMENT

A schematic showing the compound angle film hole geometry along the test surface is shown in figure 3. Here, holes are arranged in two rows which are staggered with respect to each other, with spanwise spacings between adjacent holes of 3.9d. This spanwise spacing was chosen to allow sufficient space between adjacent injection holes as the spanwise locations of vortices are changed. The distance between two adjacent holes in the same row (7.8d) is equivalent to 4.7-4.9 vortex core diameters (as measured at x/d=10.2). Determination of vortex core sizes are discussed in the next section. Figure 3 also shows that centerlines of holes in separate rows are separated by 5.2d in the streamwise direction. Each row of holes contains five injection cooling holes with a nominal inside diameter of 0.945 cm. The centerline of the middle hole of the downstream row is located on the spanwise centerline (Z=0.0 cm) of the test surface. The compound angle holes are employed with Ω=35 degrees and β=30 degrees, where Ω is the angle of the injection holes with respect to the test surface as projected into the streamwise/normal plane, and β is the angle of the injection holes with respect to the test surface as projected into the spanwise/normal plane. The plane of each injection hole is angled at 50.5 degrees from the streamwise/normal (X-Y) plane. Within the plane of each hole, hole centerlines are oriented at angles of 24 degrees from the plane of the test surface (X-Z).

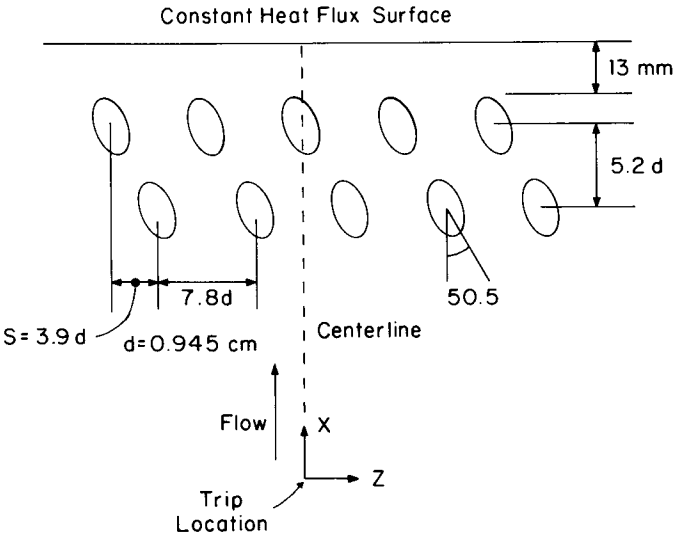

Figure 3. Injection hole arrangement along the test surface to show compound angle film cooling hole geometry.

GENERATION AND CONTROL OF VORTEX CHARACTERISTICS

The devices used to generate the vortices are shown in Fig. 4. In the present study, vortices are generated which rotate clockwise and counter-clockwise when viewed in spanwise/normal planes. In each case, each vortex generator is a half-delta wing with 3.2 cm height and 7.6 cm base. Each wing is attached to a base plate which is moved in the spanwise direction to produce vortices with different spanwise locations with respect to the film cooling holes. Delta wing arrangements used to produce clockwise-rotating vortices R0-R4, and counter-clockwise rotating vortices L0-L4 are shown in Fig. 4. The differences in the direction of vortex rotation result due to different delta wing placement on the baseplates relative to the mainstream flow direction.

With half-delta wing generators, vortices are produced with secondary flow vectors such as the ones shown in Figs. 5a and 5b. In the first of these figures, the positions of the clockwise rotating vortices R0-R4 are shown with respect to the film cooling hole locations. In the second figure, the positions of the counter-clockwise rotating vortices L0-L4 are shown with respect to the film cooling hole locations. Large arrows denote the spanwise locations of holes in the downstream row and small arrows denote the spanwise locations of holes in the upstream row. The centerline of the central injection hole (hereafter referred to as the central hole) in the downsteam row is located at Z=0.0 cm. Secondary flow vectors in Figs. 5a and 5b were measured within vortices R0 and L0, respectively, just downstream of the injection holes at x/d=10.2. The horizontal axis is then shifted in these figures so that the centerline of the central hole is appropriately oriented with respect

to vortex centers for all vortices.

Table 1 provides a tabulation of the spanwise positions of vortices R0-R4 and vortices L0-L4, as well as the vortex generators used to produce them. This includes information on the spanwise locations of vortex generator baseplates, and the locations of the central hole with respect to the vortices. The spanwise spacing between vortices R0 and R1 (as well as between vortices R1 and R2, R2 and R3, L0 and L1, L1 and L2, etc.) is 1.8 cm or 24 percent of the spacing between two adjacent holes in the same row (2s=7.8d). This is 1.14-1.18 times 2c, or just greater than the size of one vortex core diameter, where vortex core radius is denoted c. The spanwise spacing between vortices R0 and R4 and between vortices L0 and L4 are both 0.98 times 2s, or just less than the spanwise spacing between two injection holes in the same row. Table 1 also includes estimated vortex center spanwise locations. These locations were also measured (at the locations of peak streamwise vorticity) for vortices R0, R4, L0 and L4. Good agreement between measured and estimated positions is evident for all four cases, with maximum deviation of 0.42 cm for vortex L4.

At x/d=10.2, vortex core radii, c, of vortices R0-R4 and vortices L0-L4 are equal to 0.76-0.79 cm. c is determined as one half of the sum of average core radii in the Y and Z directions (as measured from vortex centers). These radii are determined for the area which encompasses all vorticity values greater than or equal to 40 percent of peak vorticity (at the center) for a particular vortex. The choice of 40 percent was made to give a good match to core radii determined at the locations of maximum secondary flow vectors. The area enclosed by secondary flow maxima is important, because for ideal Rankine vortices, it corresponds to the ideal core which contains all vorticity. Secondary flow vector maxima are not used to determine core size as this gives results which are less accurate than the 40 percent threshold approach. 2c/d then gives the ratio of vortex core diameter to injection hole diameter. At x/d=10.2, this quantity is then about 1.6-1.67 for vortices R0-R4 as well as for vortices L0-L4.

Referring to Fig. 5a and Table 1, with vortex R0, the central hole is located beneath the vortex downwash. With vortex R1, the central hole is located beneath the vortex core near the downwash. Upwash regions of vortices R2 and R3 are located above the central hole, whereas vortex R4 passes injection locations such that the central hole lies to the side of the upwash. Vortices R0 and R4 are displaced a spanwise distance from each other which about equals the spanwise spacing between two injection holes in the upstream row (7.8d). Thus, even though these two vortices are at different positions with respect to the central hole, they are at about the same positions relative to the hole placement pattern in upstream and downstream rows because of the spanwise periodicity of the injection hole locations. Consequently, spanwise variations of local heat transfer distributions are expected to be about the same for vortices R0 and R4 except for spanwise displacement of 7.8d or 7.37 cm.

In Fig. 5b, it is evident that vortex L0 is located so that its downwash passes above the the central hole as it passes x/d=0.0. With vortex L1, the central hole is located beneath the vortex core near the downwash. Upwash regions of vortices L2 and L3 are located above the central hole, whereas vortex L4 passes injection locations such that the central hole lies to the side of the upwash. Compared to vortices R0-R4, vortices L0-L4 from a mirror image with repect to the Z axis. Just as for vortices R0 and R4, vortices L0 and L4 are displaced a spanwise distance from each other which about equals the spanwise spacing between two injection holes in the upstream row (7.8d). Thus, even though vortices L0 and L4 are at different positions with respect to the central hole, they are at about the same positions relative to the hole placement pattern. Consequently, local heat transfer distributions are expected to be about the same for vortices L0 and L4 except for spanwise displacement of 7.8d or 7.37 cm.

Circulation magnitudes are calculated assuming that all vorticity values less than a threshold are equal to zero. The same numerical threshold of 100. (1/s) is used throughout this paper, chosen arbitrarily. It is about equal to 11 percent of the maximum vorticity of vortex R0 at x/d=10.2 with no injection (909.8 1/s). At x/d= 10.2, circulation magnitudes (with no film cooling) range from 0.171 m^2/s to 0.177 m^2/s for vortices R0-R4, and from

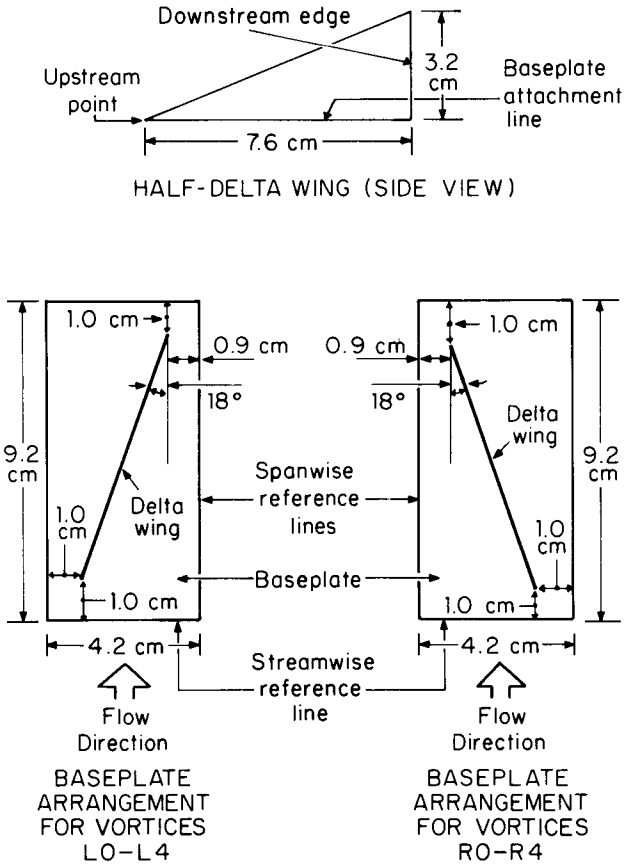

Figure 4. Vortex generator geometries and orientations to produce clockwise and counter-clockwise vortices (as viewed in spanwise/normal planes). Also shown are the dimensions of the vortex generator delta wing.

0.149 m^2/s to 0.156 m^2/s for vortices L0-L4. Higher levels of vorticity evidence larger gradients of secondary flow vectors as one moves away from the vortex center. As vortex circulation becomes larger, secondary flow velocities between the main vortex center and wall increase, and amounts of spanwise vortex drift increase as the vortices are convected downstream.

With film injection at a blowing ratio of 0.5, parameter S (= Γ/U_c d) ranges from 3.62 to 3.75 for vortices R0-R4, and from 3.15 to 3.30 for vortices L0-L4. Parameter S1 (= Γ/U_c 2c) ranges from 2.19 to 2.24 for vortices R0-R4, and from 1.96 to 1.99 for vortices L0-L4. These two parameters give measures of vortex strength relative to the injection velocity from measurements at x/d=10.2 (Ligrani et al., 1991). According to Ligrani et al. (1991), S values higher than 1-1.5 and S1 values higher than 0.7-1.0 produce situations with simple angle film cooling in which injectant is swept into the vortex upwash and above the vortex core by secondary flows, and local heat transfer measurements show evidence of injectant beneath vortex cores and downwash regions near the wall only for x/d up to 17.4.

HEAT TRANSFER AND INJECTANT DISTRIBUTIONS

In the discussion which follows, results with vortices R0-R4 are presented in Figs. 6-9, and results with vortices L0-L4 are presented in Figs. 10-11. Information on the streamwise development of local Stanton numbers with m=0.5 film cooling are presented in Fig. 12 for vortex R0 and in Fig. 13 for vortex L0.

Heat transfer and injectant distributions with vortices R0-R4.

Distributions of St/Sto as dependent upon spanwise coordinate Z

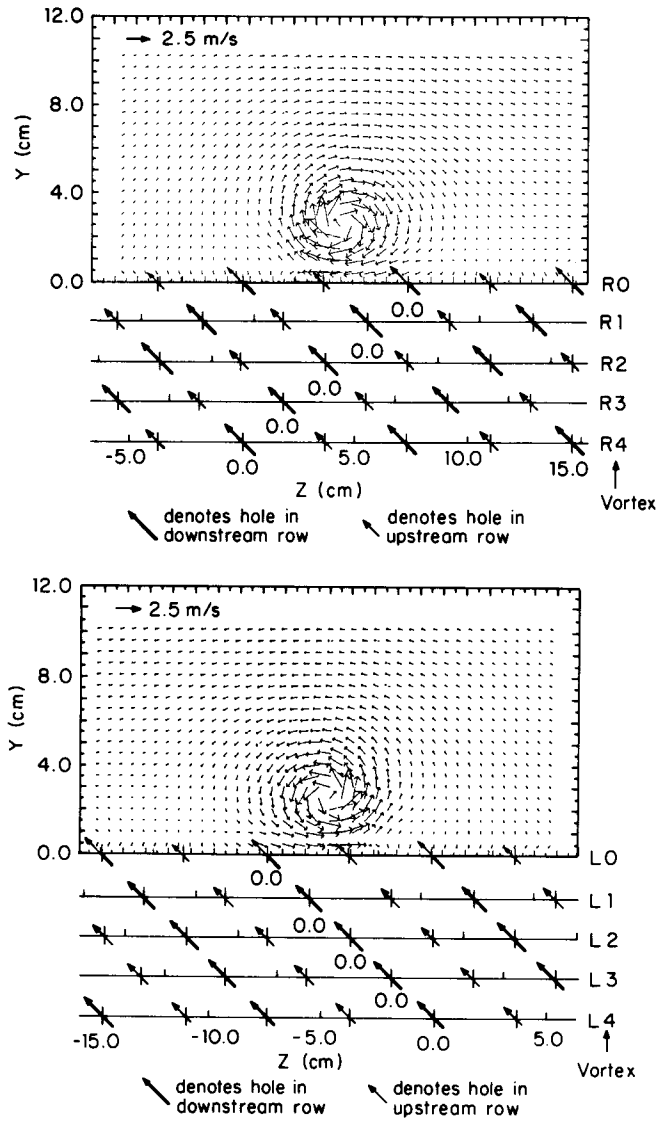

Figure 5. Film cooling injection locations with respect to vortex center and secondary flow vectors (x/d=10.2) (a) for vortices R0-R4, and (b) for vortices L0-L4. Each horizontal scale corresponds to a different vortex and different spanwise vortex position where Z=0 corresponds to the centerline of the injection hole located on the wind tunnel centerline.

are presented in Fig. 6. These data were measured at x/d=33.1 (X=1.377 m) with film injection from both rows of holes at a blowing ratio m of 0.5 both with and without longitudinal vortices R0-R4 embedded in the turbulent boundary layer.

In the top portion of Fig. 6, St/Sto distributions are presented for vortices R0 and R4 along with Stf/Sto data obtained when no vortices are present in the flow. Of the features on this portion of Fig. 6, most apparent are the disturbances to local St/Sto distributions which result from the vortices. This is apparent where St/Sto > Stf/Sto, which occurs for Z > -7 cm for vortex R0 and for Z > 0 cm for vortex R4 as a consequence of the proximity of vortex downwash regions to these parts of the test surface. Here, St/Sto values are as high as 1.05 compared to Stf/Sto values from 0.80 to 0.85, where the latter are measured when no vortices are present. Test surface locations beneath vortex upwash regions correspond to Z < -7 cm for vortex R0 and to Z < 0 cm for vortex R4. Here, St/Sto values are generally lower than the Stf/Sto distribution.

The spanwise variations of local heat transfer are about the same for vortices R0 and R4 except for spanwise displacement with respect to each other a distance of about 7.2 cm. This validates the measurement apparatus and procedures employed to obtain local heat transfer distributions. The small quantitative differences between the two curves which occur locally result because of the strong dependence of local heat transfer distributions on the positions of the embedded longitudinal vortices as they pass the injection holes, and the fact that the spanwise displacement between the two vortices is slightly less than 2s, the spanwise spacing between two adjacent holes in the downstream row. In this case the vortices are displaced from each other a distance of 7.2 cm or 98 percent of 2s (Table 1).

St/Sto distributions with vortices R0, R1, R2 and R3 are presented in the bottom portion of Fig. 6. Here, significant quantitative and qualitative variations are seen as the spanwise locations of the vortices are changed. When the St/Sto distributions are compared to each other, significant changes to the shapes of local maxima as well as to surrounding heat transfer distributions are apparent. Such variations evidence complicated interactions as the vortices interact simultaneously with injectant from several injection holes. One important similarity caused by all four vortices is the sharp spanwise gradient of St/Sto which apparent at Z from -5 cm to 2 cm. As expected, this gradient moves in the +Z direction as the spanwise locations of the vortices move in the +Z direction. Away from this gradient, St/Sto values approach Stf/Sto both as large Z and at small Z at locations where the influences of the embedded vortices become less important. The highest local St/Sto value occurs with vortex R2 which convects downstream so that its core and upwash region pass over the central injection hole at Z=0

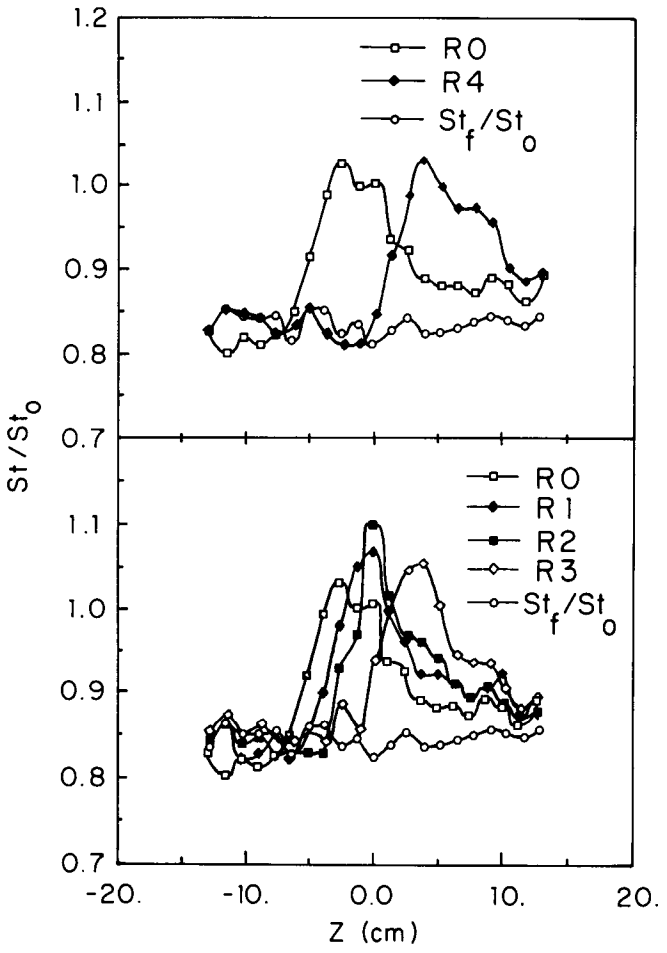

Figure 6. Spanwise variations of local Stanton number ratios at x/d = 33.1 with m=0.5 film cooling both with and without clockwise rotating vortices R0-R4 . Freestream velocity = 10 m/s. Vortex spanwise positions and locations with respect to film injection holes are given in Table 1.

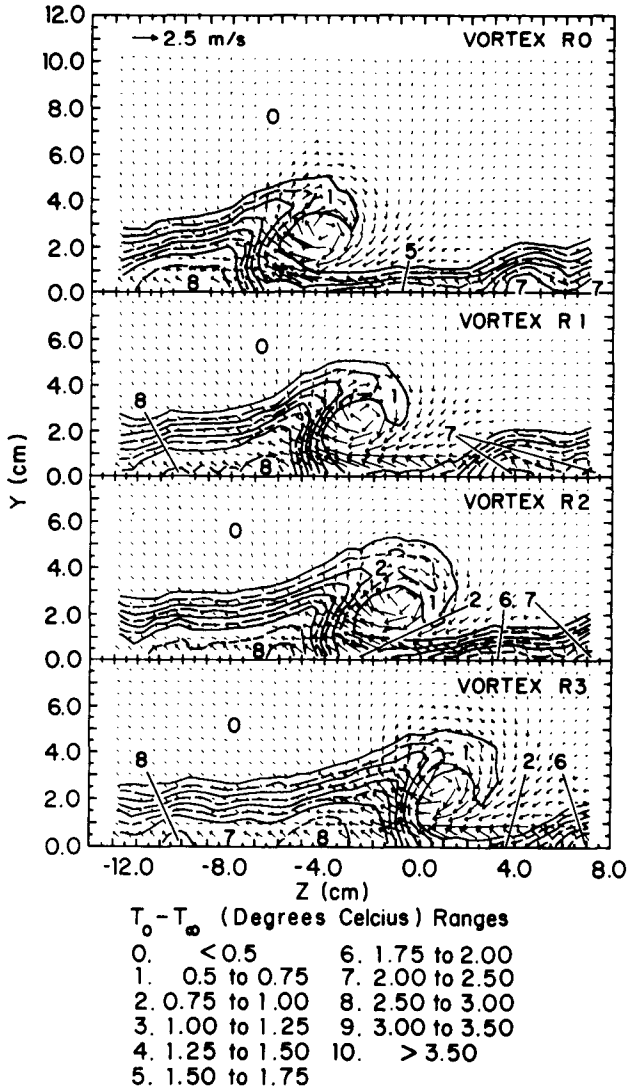

Figure 7. Mean temperature field showing distributions of film injectant with secondary flow vectors at x/d = 45.8, with m=0.5 film cooling and a freestream velocity of 10 m/s. Data are given for clockwise rotating vortices R0-R4. Vortex spanwise positions and locations with respect to film injection holes are given in Table 1.

cm. This situation is similar to one observed by Ligrani et al. (1989a) for injection from holes with simple angle orientations. In that study, the greatest disturbances to injectant occur when the vortex core passes over a film cooling hole, compared to situations in which the vortex core passes between two injection locations (ie. vortices R1 and R3). According to Ligrani and Williams (1990), significant perturbations to injectant distributions (from simple angle holes) result when vortex cores pass within 1.67 core diameters on the downwash side, and 0.87 core diameters on the upwash side. The only vortices which meet this criteria with respect to the central hole are R1 and R2. However, the Ligrani and Williams (1990) criteria is expected to be somewhat different when compound angle injection is employed.

Fig. 7 quantifies the distortion and rearrangement of injectant by vortices R0-R3. These data are given for a blowing ratio m of 0.5 at x/d=45.8. As mentioned earlier, the spanwise locations of vortices R0-R3 with respect to the film cooling holes are given in Fig. 5a and Table 1. From these two sources, it is evident that either downwash regions (vortices R0 and R1), core regions (vortices R1 and R2), or upwash regions (vortices R2 and R3) pass over the central injection hole as the vortices are convected downstream.

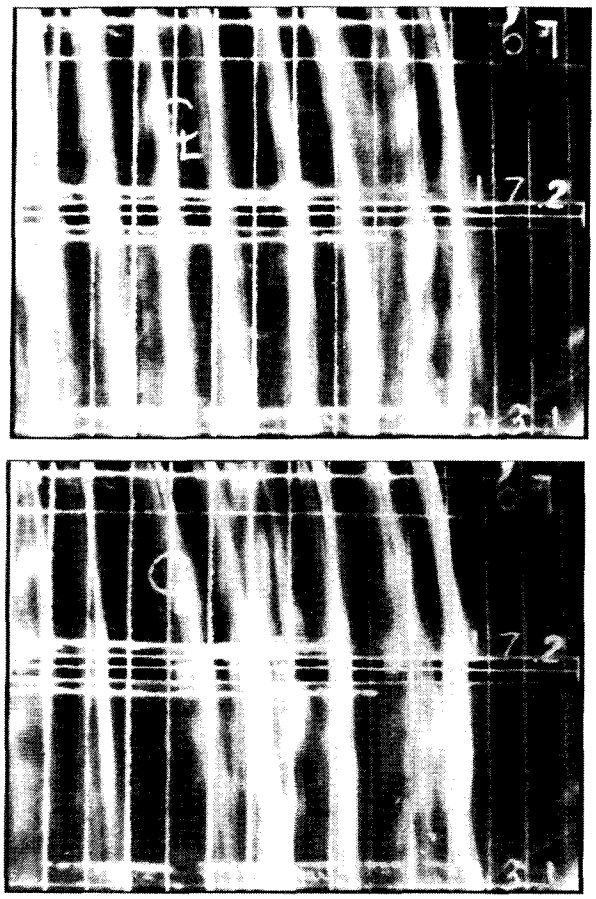

Figure 8. Photographs of flow along the test surface which show distributions of injectant contaminated by fog fluid in streamwise/spanwise planes. The bulk flow (or streamwise direction) is down the page, and the spanwise direction is across the page. (a) No vortex and m=0.5 film cooling. (b) Vortex R1 and m=0.5 film cooling.

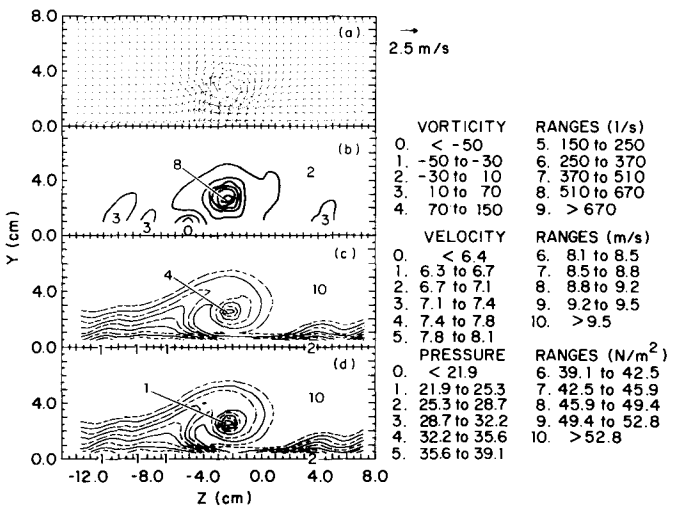

Figure 9. Distributions of (a) secondary flow vectors, (b) streamwise vorticity, (c) streamwise mean velocity, and (d) total pressure with vortex R1 and film cooling at m=0.5 as measured at x/d=45.8 with a freestream velocity of 10 m/s.

Measured secondary flow vectors are superimposed on each part of Fig. 7 to illustrate how their magnitudes and distributions relate to the reorganization of injectant by the different vortices. The same scaling for secondary flow vectors is used throughout all parts of Fig. 7. Procedures to determine injectant distributions were developed by Ligrani, et al (1989a) and later also used by Ligrani and Williams (1990). In these studies and the present one, injectant distributions are qualitatively correlated to mean temperature distributions. To do this, injectant is heated to 50 degrees Centigrade without providing any heat to the test plate. Thus, because the injectant is the only source of thermal energy (relative to freestream flow), higher temperatures (relative to freestream temperature) generally indicate greater amounts of injectant. The temperature field is therefore given as $(T-T_\infty)$, and as such, shows how injectant accumulates and is rearranged mostly as a result of convective processes from the boundary layer and vortex secondary flows. Diffusion of injectant heat accounts for some of the temperature variations observed between injection hole exits and measuring stations, but compared to convection, this is of secondary importance.

If no vortex is present, concentrations of injectant are present in the boundary layer near the wall spaced about 3.7 cm apart in the spanwise direction at the same interval as the injection hole spacing. In Fig. 7, it is evident that all four vortices R0-R3 result in significant disturbances to the injectant because the distributions shown are different from the ones which would exist if no vortices are present. In each case, injectant is swept beneath the vortex centers in the negative Z direction, then into vortex upwash regions, and finally above the vortex centers. The spanwise locations of the centers of vortices R0, R1, R2 and R3 at x/d=45.8 are at Z equal to -4.06 cm, -2.54 cm, -0.51 cm, and 1.52 cm, respectively. The Y coordinate of vortex centers is 2.5-2.6 cm. Centers are located at the point of maximum streamwise vorticity and are apparent in Fig. 7 at locations around which secondary flow vectors swirl.

Except for spanwise displacement, overall injectant distributions for vortices R0-R3 in Fig. 7 show some qualitative similarity. This is partially a result of the small spacing between holes in the spanwise direction which results in abundant amounts of injectant at locations just downstream of x/d=0.0. The small quantitative differences between the different injectant distributions result as different portions of different vortices interact with injectant from different film cooling holes as the vortices pass x/d=0. Important injectant deficits are present in Fig. 7 beneath vortex cores, and near vortex cores beneath downwash regions because of the influences of vortex secondary flows. These deficits correspond to locally higher St/Sto values in Fig. 6 at the same Z locations. Injectant deficits are most severe for vortices R1 and R3 at respective Z locations of -4.0 cm to 0.0 cm, and 0.0 cm to 4.0 cm. The corresponding local maxima in Fig. 6 are large and broad and cover the same ranges of Z.

The redistribution of injectant by vortex R1 is further illustrated by the two photographs in Fig. 8. Each shows a plan view of the test surface (ie. a streamwise /spanwise plane view) such that the streamwise direction is down the page, and the spanwise direction is across the page. Vertical white lines along the test surface in each photograph are spaced 2.54 cm apart in the spanwise direction, with the line along the spanwise centerline labelled accordingly. Horizontal lines are apparent at x/d of 6.7, 17.2, and 33.1. The injectant, which is contaminated with fog fluid, is clearly apparent in each photograph as it is convected downstream. For both cases, the injectant emerges from the two staggered rows of holes at a blowing ratio m of 0.5.

The top photograph of Fig. 8 shows flow along the test surface when no vortex is present, and the bottom one shows how the injectant is rearranged and distorted as vortex R1 is convected downstream. In the top photograph, injectant from each hole is immediately adjacent to injectant from neighboring holes across the span of the view shown. Slight spanwise components of injectant velocity are apparent near x/d=6.7. As the smoke convects farther downstream, slight turning into the streamwise direction is apparent. However, the smoke continues to move at a slight angle with respect to the streamwise direction at x/d even as large as 33.1, as shown in the bottom portion of the photograph.

Similar behavior is evident in the bottom photograph of Fig. 8 except for significant disruptions of injectant by vortex R1. These are most apparent just to the left of the spanwise centerline for x/d from 6.7 to 17.2, and along the spanwise centerline for x/d from 17.2 to 33.1. At these locations, the scarcity of fog fluid evidences little injectant along the test surface. Such regions correspond to vortex downwash regions and regions beneath vortex cores, where St/Sto distributions like the ones in Fig. 6 show locally higher values compared to nearby magnitudes. Just to the right of the injectant deficits (ie. at smaller Z), extra accumulations of injectant are apparent in Fig. 8 as a consequence of convection by secondary flows within upwash regions of vortex R1. In some cases, such extra accumulations of injectant result in local increases of film protection where values of St/Sto are locally lower than values of Stf/Sto which would exist if no vortex were present. At x/d=33.1, the injectant in the bottom photograph of Fig. 8 is deficit at Z from -2.5 cm to 2.5 cm, with extra accumulations at Z from -7.6 cm to -2.5 cm. These values are consistent with injectant distributions in Fig. 7 for vortex R1 at x/d=45.8 considering the negative spanwise convection of the vortex between the two streamwise locations. In the latter case, deficits of injectant are apparent along the wall at Z from -3.5 cm to 1.5 cm, and extra accumulations are apparent along the wall at Z from -8.5 cm to -3.5 cm.

Examples of flow properties measured in streamwise/normal planes at x/d=45.8 with vortex R1 and m=0.5 film cooling are presented in Fig. 9. These include secondary flow vectors, streamwise vorticity distributions, distributions of streamwise mean velocity, and distributions of mean total pressure. In part a, the rotation of the clockwise vortex is clearly apparent about the vortex center located at Y=2.48 cm and Z=-2.54 cm. The center corresponds to the location of maximum streamwise vorticity which is clearly apparent in part b. The contours of streamwise vorticity which surround this center are approximately circular in shape with a region of negative vorticity located near the wall at Z from -4.0 cm to -6.0 cm (ie. just to the left of the main vortex). Streamwise vorticity magnitudes are determined from secondary flow vector magnitudes using a finite difference form of the equation given by $\partial U_Y/\partial Z - \partial U_Z/\partial Y$. Distributions of streamwise mean velocity and total pressure in respective parts c and d of Fig. 9 are qualitatively similar. In both cases, a region where these quantities are locally higher is present near the wall within the vortex downwash. In addition, a region of low velocity and low pressure is present away from the wall within the vortex upwash, and deficits of velocity and pressure are present near the center of the vortex. Horizontal contour lines in parts c and d of Fig. 9 provide clear evidence of the turbulent boundary layer located on either side of the vortex. Within the boundary layer, additional deficits of pressure and velocity are present along the wall at locations of film injectant accumulation.

Heat transfer and injectant distributions with vortices L0-L4.

In the discussion which follows, surface heat transfer results with vortices L0 and L4 are discussed first. This is followed by discussions of St/Sto results obtained with vortices L0-L4, and then by comparisons of these results with ones for vortices R0-R4. Injectant distributions for vortices L0-L4 are then discussed last.

Spanwise distributions of St/Sto measured both with and without longitudinal vortices L0-L4 embedded in the turbulent boundary layer are shown in Fig. 10. As for the results shown in Fig. 6, the data in Fig. 10 were measured at x/d=33.1 (X=1.377 m) with film injection from both rows of holes at a blowing ratio m of 0.5. In the top portion of Fig. 10, St/Sto distributions are presented for vortices L0 and L4 along with Stf/Sto data obtained when no artificially induced vortices are present in the flow. As for the results in the top of Fig. 6, the ones in the top of Fig. 10 illustrate significant disturbances to local St/Sto distributions because of the vortices. This is particularly apparent in Fig. 10 for -5 cm < Z < 4 cm for vortex L0, and for Z < -4 cm for vortex L4 if the St/Sto distributions are compared to the Stf/Sto distribution obtained with no vortices in the flow. St/Sto are higher than Stf/Sto over these areas as a consequence of the proximity of vortex downwash regions to these portions of the test surface. Vortex secondary flows within

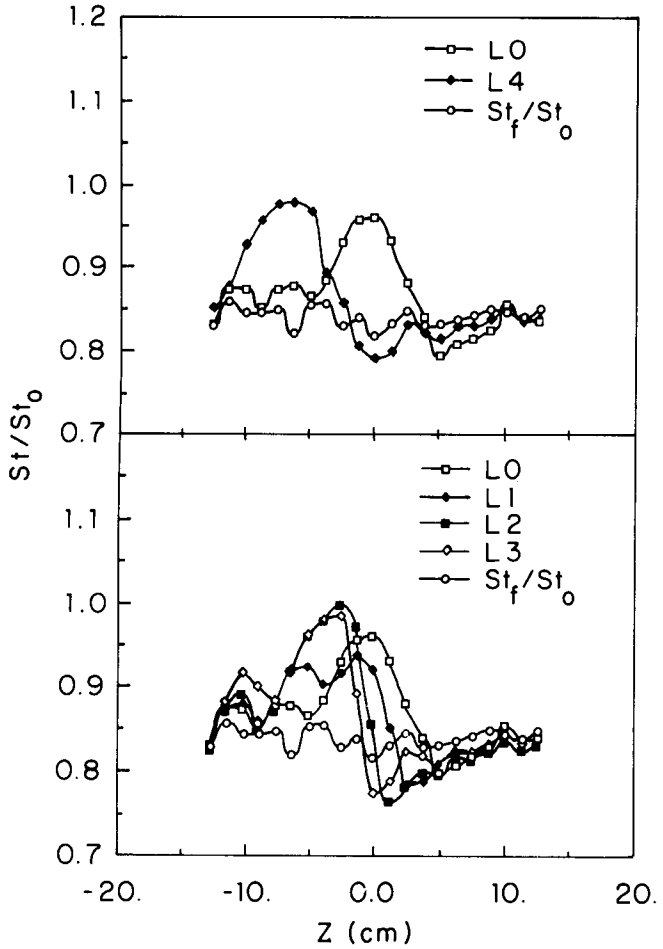

Figure 10. Spanwise variations of local Stanton number ratios at x/d = 33.1 with m=0.5 film cooling both with and without counter-clockwise rotating vortices L0-L4 . Freestream velocity = 10 m/s. Vortex spanwise positions and locations with respect to film injection holes are given in Table 1.

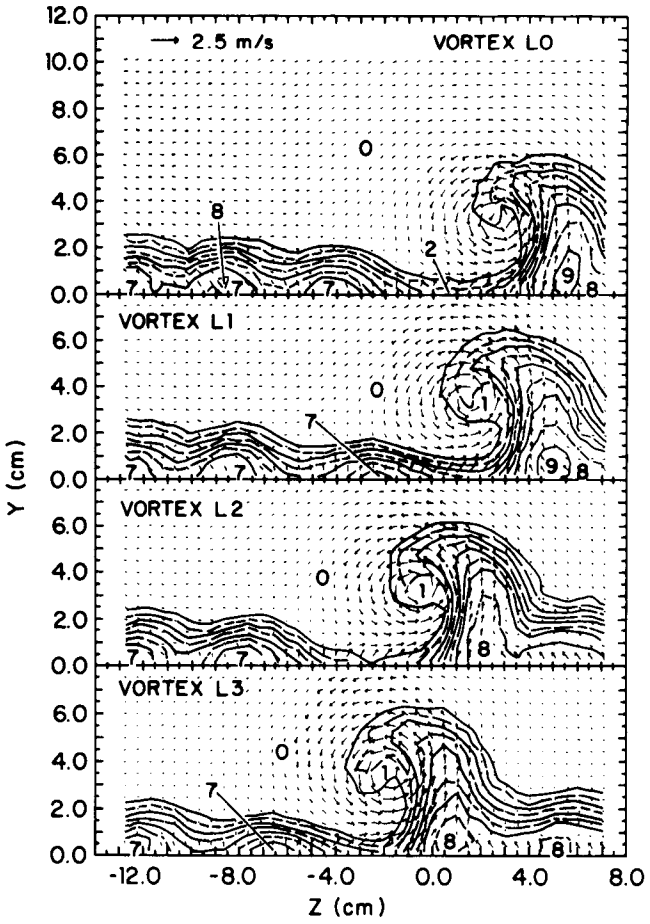

Figure 11. Mean temperature field showing distributions of film injectant with secondary flow vectors at x/d = 45.8, with m=0.5 film cooling and a freestream velocity of 10 m/s. Data are given for counter-clockwise rotating vortices L0-L4. Vortex spanwise positions and locations with respect to film injection holes are given in Table 1.

downwash regions and beneath vortex cores first sweep injectant in the spanwise direction along the wall and then into upwash regions. Deficits of injectant then result beneath downwash regions which give decreased protection, and increased St/Sto relative to Stf/Sto. The top portion of Fig. 10 also shows that St/Sto values for each vortex are generally lower than the Stf/Sto distribution for Z larger than 4 cm for vortex L0 and for Z larger than -4 cm for vortex L4. These locations correspond to regions beneath vortex upwash regions where extra injectant accumulates resulting in local increases of protection by the film.

The spanwise variations of local heat transfer are about the same for vortices L0 and L4 except for spanwise displacement with respect to each other a distance of about 7.2 cm, which is equivalent to 98 percent of 2s (Table 1). This provides validation of the measurement apparatus and procedures employed to obtain local heat transfer distributions in addition to that given by results in the top of Fig. 6. The small quantitative differences between the curves for vortices L0 and L4 in the top of Fig. 10 occur locally for the same reasons that data for vortices R0 and R4 in the top of Fig. 6 are locally different.

St/Sto distributions with vortices L0, L1, L2 and L3 are presented in the bottom portion of Fig. 10. Here, significant quantitative and qualitative variations are seen as the spanwise locations of the vortices are changed. When the St/Sto distributions are compared to each other, significant changes to the shapes of local maxima as well as to surrounding heat transfer distributions are apparent. Just like the results in Fig. 6, such variations evidence complicated interactions as the vortices interact simultaneously with injectant from several injection holes. In addition, vortices L0-L4 also result in sharp spanwise gradients of St/Sto. In Fig. 10, these gradients are apparent at Z from -2 cm to 4 cm, and move in the -Z direction as the spanwise locations of the vortices move in the -Z direction. The highest local St/Sto value just to the left of one such gradient (ie. at smaller Z) occurs with vortex L2. This particular vortex convects downstream so that its core and upwash region pass over the central injection hole at Z=0 cm (ie. Fig. 5b and Table 1).

Vortices L0-L4 are different from vortices R0-R4 because of different directions of rotation (counter-clockwise versus clockwise) when viewed looking downstream in spanwise/normal planes. This is important because secondary flow vectors, especially beneath vortex cores, are in different directions with respect to the spanwise coordinate Z as well as with respect to spanwise velocity components of injectant. Fig. 3, which shows the orientations of the film cooling holes with respect to streamwise and spanwise coordinate directions, indicates the latter to be in the -Z direction. In Fig. 5a, secondary flow vectors near the wall for vortices R0-R4 are then in the same direction as the spanwise components of the injectant velocity. The opposite is true in Fig. 5b, where the near-wall secondary flow vectors for vortices L0-L4 have directions which are opposite to the direction of the spanwise components of the injectant velocity.

These differences between vortices R0-R4 and vortices L0-L4 are important because they result in significantly different local

St/Sto distributions as the vortices interact with the film injectant. This is evident if St/Sto for vortices R0-R4 in Fig. 6 are compared to ones in Fig. 10 for vortices L0-L4. This comparison can be made for the same locations of vortex centers with respect to the central film injection hole with the only changes due to the direction of rotation of the vortices. It is evident from Figs. 5a and 5b and Table 1 that this is done by comparing results for vortices having the same numbers in their name labels (ie. comparing results for vortex R0 with results for vortex L0, comparing results for vortex R1 with results for vortex L1, R2 with L2, etc.). Because they are the same in all parts of Figs. 6 and 10, Stf/Sto distributions (with film injection and no vortices) are appropriate to use in reference to distributions measured with vortices R0-R4 and L0-L4.

With each comparison, the same overall qualitative difference between the clockwise and counter-clockwise vortices is evident. St/Sto distributions with the clockwise rotating vortices R0-R4 always show regions greater than Stf/Sto over larger portions of the test surface than the St/Sto distributions associated with counter-clockwise rotating vortices L0-L4. In addition, St/Sto distributions with vortices R0-R4 show higher local maxima and maxima peaks which are broader and spread over greater areas compared to St/Sto measured beneath vortices L0-L4. Such differences evidence different interactions between injectant and the two types of vortices. Higher St/Sto are present with vortices R0-R4 because the injectant is swept away from the wall (which results in decreased protection) more efficiently than with vortices L0-L4. The more efficient decimation of the injectant occurs since near-wall vortex secondary flows are in the same direction as the spanwise velocity components of the injectant. With vortices L0-L4, the opposite situation is present. Here, near-wall vortex secondary flows oppose the spanwise components of the film injectant resulting in greater resistance to injectant rearrangement by the vortices.

Fig. 11 quantifies the distortion and rearrangement of injectant by vortices L0-L3. These data were obtained for a blowing ratio m of 0.5 at x/d=45.8 using the same procedures employed to obtain the injectant distributions and secondary flow vectors given in Fig. 7. The spanwise locations of vortices L0-L3 with respect to the film cooling holes are given in Fig. 5b and Table 1. From these two sources, it is evident that either downwash regions (vortices L0 and L1), core regions (vortices L1 and L2), or upwash regions (vortices L2 and L3) pass over the central injection hole as the vortices are convected downstream.

Like the results presented in Fig. 7, the injectant distributions in Fig. 11 show that all four vortices L0-L3 produce significant disturbances to the injectant relative to distributions present if no vortices are present. Individual distributions in Fig. 11 are qualitatively similar to each other, except for variations due to spanwise displacement of the vortices with respect to the film injection holes. They also show some qualitatively similarity to the ones in Fig. 7. The most important differences result because of different directions of vortex rotation. With vortices L0-L4, this causes much more injectant to be present next to the wall near the vortices, which is apparent if regions just to the right of vortex downwash regions in Fig. 7 are compared to regions just to the left of vortex downwash regions in Fig. 11. Such differences are particularly evident if the injection distribution for vortex L0 is compared ot the one for vortex R0.

In Fig. 11, injectant is swept beneath the vortex centers in the positive Z direction, then into vortex upwash regions, and finally above the vortex centers. The spanwise locations of the centers of vortices L0, L1, L2 and L3 are at Z equal to 3.05 cm, 1.52 cm, -0.51 cm, and -1.52 cm, respectively. The Y coordinate of vortex centers in Fig. 11 vary from 2.9 cm to 3.0 cm. In each case, injectant deficits are present near the wall in Fig. 11 located beneath vortex cores and near vortex cores beneath downwash regions. Of these, the most severe are located beneath vortices L0 and L2 at respective Z locations of 0.0 cm to 4.0 cm, and -4.0 cm to 0.0 cm. Corresponding St/Sto distributions in Fig. 10 show broad local maxima over nearly the same ranges of Z.

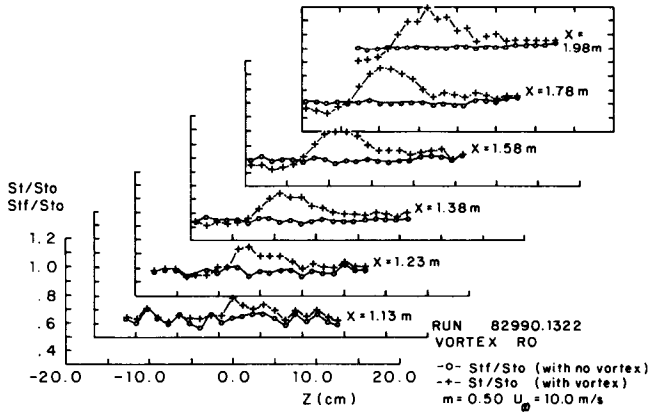

Figure 12. Streamwise development of Stanton number ratios with m= 0.5 film cooling both with and without vortex R0. With this clockwise rotating vortex, the downwash passes over the central film cooling hole. Freestream velocity = 10 m/s.

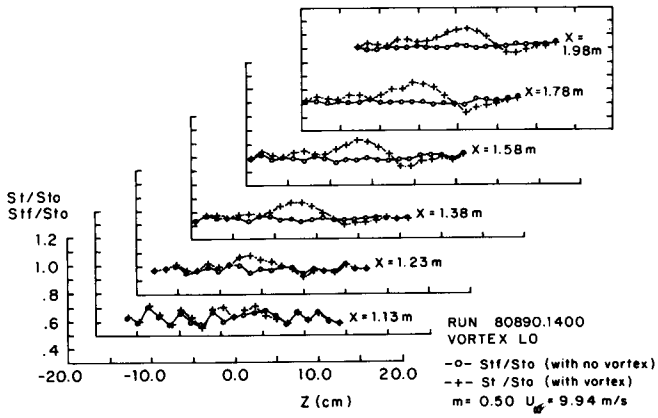

Figure 13. Streamwise development of Stanton number ratios with m= 0.5 film cooling both with and without vortex L0. With this counter-clockwise rotating vortex, the downwash passes over the central film cooling hole. Freestream velocity = 10 m/s.

Streamwise development of heat transfer distributions with film cooling both with and without vortices R0 and L0.

Streamwise development of local St/Sto distributions with longitudinal vortices R0 and L0 are presented in Figs. 12 and 13, respectively. Also included on these figures are distributions of Stf/Sto obtained with film cooling only and no vortices embedded in the boundary layers. These two sets of results are presented together in each figure so that disturbances caused by the vortices to surface heat transfer in the film cooled boundary layers are apparent. In both figures, results are given for a blowing ratio m of 0.5 and a freestream velocity of 10 m/s.

In examining results on Figs. 12 and 13, it is apparent that the disturbances caused by the vortices persist to the end of the test plate. This is evident since St/Sto values are higher than Stf/Sto at X=1.98 m or x/d=96.6. In fact, differences between St/Sto and Stf/Sto generally become greater with streamwise development, behavior which illustrates the coherence of the vortices as they are convected downstream. Differences are quite small just downstream of the injection holes at X=1.13 m or x/d=6.7, which indicates that the film, rather than the vortices, are most affecting local heat transfer behavior at this location. According to Ligrani et al. (1989a), such behavior probably results because the vortices are lifted off of the test surface by the film injectant. In addition, vortex secondary flows have not had enough time to rearrange the injectant at this streamwise station since it is just downstream of film hole exit locations, where the vortices initially interact with the

injectant.

Comparing results in Fig. 12 to ones in Fig. 13 reveals important differences for vortices R0 and L0. In Fig. 12, regions where St/Sto are higher than Stf/Sto are at larger Z, and regions where St/Sto are lower than Stf/Sto are at smaller Z. The opposite trend is present in Fig. 13 because vortex L0 rotates in a direction opposite to vortex R0. However, in spite of these differences, both vortices R0 and L0 produce St/Sto > Stf/Sto beneath downwash regions, and St/Sto < Stf/Sto beneath upwash regions. Greater disturbances and higher St/Sto are present beneath the downwash regions of vortex R0 because injectant is swept away from the wall more efficiently than occurs with vortex L0. This is because near-wall secondary flows of vortex R0 are coincident with the spanwise velocity components of the film injectant. As mentioned earlier, this results in larger reductions in protection than if the secondary flows of a vortex are opposite to the spanwise component of injectant velocity, as with vortex L0. Regions where St/Sto are greater than Stf/Sto also cover larger spanwise portions of the test plate with vortex R0. This is consistent with the St/Sto results in Figs. 6 and 10. It is also consistent with the injectant distributions in Figs. 7 and 11, which show that injectant is present much closer to the downwash regions of vortices L0-L4 than to the downwash regions of vortices R0-R4.

SUMMARY AND CONCLUSIONS

Experimental results are presented which describe the effects of embedded, longitudinal vortices on heat transfer and film injectant downstream of two staggered rows of film cooling holes with compound angle orientations. Holes are oriented so that their angles with respect to the test surface are 30 degrees in a spanwise/normal plane projection, and 35 degrees in a streamwise/normal plane projection. A blowing ratio of 0.5, non-dimensional injection temperature parameter θ of about 1.5, and freestream velocity of 10 m/s are employed. Injection hole diameter is 0.945 cm to give a ratio of vortex core diameter to hole diameter of 1.6-1.67 just downstream of the injection holes (x/d=10.2). At the same location, vortex circulation magnitudes range from 0.15 m^2/s to 0.18 m^2/s. With film injection at a blowing ratio of 0.5, the ratio of vortex circulation to injection velocity times hole diameter ($S = \Gamma/U_c\ d$) then ranges from 3.2 to 3.8, and the ratio of vortex circulation to injection velocity times vortex core diameter ($S1 = \Gamma/U_c\ 2c$) ranges from 2.0 to 2.2.

The most important major conclusion is that local heat transfer and injectant distributions are strongly affected by the longitudinal embedded vortices, including their directions of rotation and their spanwise positions with respect to film injection holes. Vortices are generated using half-delta wings attached to the test surface of the wind tunnel at 18 degree angles of attack with respect to the mainstream flow direction. By changing the sign of the angle of attack, vortices are produced which rotate either clockwise or counter-clockwise when viewed looking downstream in spanwise/normal planes. By moving the delta wings in the spanwise direction, the spanwise locations of the vortices with respect to the film cooling holes are also changed.

Differences resulting from vortex rotation are due to secondary flow vectors, especially beneath vortex cores, which are in different directions with respect to the spanwise velocity components of injectant after it exits the holes. When secondary flow vectors near the wall are in the same direction as the spanwise components of the injectant velocity (clockwise rotating vortices R0-R4), the film injectant is readily swept beneath vortex cores and into vortex upwash regions. Consequently, the protection provided by the injectant is reduced significantly and St/Sto may be as large as 1.05 compared to Stf/Sto values with no vortex from 0.80 to 0.85. With the opposite situation (counter-clockwise rotating vortices L0-L4), the secondary flow vectors near the wall are directed opposite to the direction of the spanwise components of the injectant velocity, and the injectant is less likely to be rearranged by vortex secondary flows. As a result, higher St/Sto are present over larger portions of the test surface with vortices R0-R4 because the injectant is swept away from near wall regions (which results in decreased protection) more efficiently than with vortices L0-L4. Because of the design of the present experiment, these comparisons are made for the same locations of vortex centers with respect to the central film injection hole (located at Z/d=0.0) such that the only changes are due to the direction of vortex rotation. With this type of comparison, St/Sto distributions with vortices R0-R4 show higher local maxima and maxima peaks which are broader and spread over greater areas compared to St/Sto measured beneath vortices L0-L4. Such behavior is consistent with injectant distribution surveys, which show larger quantities near the wall in proximity to vortices L0-L4, especially on the sides of vortex downwash regions away from the vortex centers.

A second major conclusion pertains to the compound angle orientations of the injection holes. Because of this, disruptions to the injectant and heat transfer caused by the vortices are different from the disruptions which result when similar vortices interact with injectant from holes with simple angle orientations. Ligrani, et al. (1991) present results measured downstream of a single row of simple angle holes inclined at 30 degrees with respect to the test surface and spaced 3.0 diameters apart in the spanwise direction. St/Sto results are given for a blowing ratio of 0.5 with slightly weaker vortices than employed in the present study (vortex circulation magnitudes range from 0.13 m^2/s to 0.15 m^2/s, S = 1.58-1.61, S1 = 1.75-1.78). Relative to Stf/Sto distributions for x/d = 33.1, the Ligrani, et al. (1991) St/Sto maxima are higher than the present results with counter-clockwise rotating vortices (L0-L4), and lower than the present results with clockwise rotating vortices (R0-R4). Such behavior indicates that magnitudes of St/Sto maxima are qualitatively related to the angle between the injectant along the plane of the test surface and the direction of vortex secondary flow vectors near the wall (ie. the spanwise or Z direction). With this dependence, smaller angles lead to greater disruptions to nominal injectant distributions and larger decreases in protection.

If one considers either the clockwise vortices or the counter-clockwise vortices by themselves, significant St/Sto variations are seen as the spanwise positions of the vortices are changed. These result because different portions of different vortices interact with injectant from different film cooling holes as the vortices pass x/d=0. Alterations resulting from different spanwise vortex positions include changes to local St/Sto maxima and to surrounding heat transfer distributions, as well as changes to injectant distributions measured in spanwise/normal planes. When near-wall vortex secondary flow vectors oppose the spanwise component of the injectant (vortices L0-L4), local St/Sto maxima are lowest when either the downwash or core pass over the central injection hole at Z=0 cm (vortices L0 and L1). When near-wall vortex secondary flow vectors are coincident with the spanwise component of the injectant (vortices R0-R4), local St/Sto maxima are lowest when core regions of the vortices pass between injection holes in the downstream row of holes (vortices R0 and R3).

However, in spite of these quantitative variations, many overall qualitative features remain the same as the spanwise position of a vortex is changed. These include significant deficits of injectant beneath vortex cores, as well as near vortex cores beneath downwash regions, which always correspond to St/Sto values which are locally higher than Stf/Sto values at the same x/d and Z locations. Such variations persist as far as 97 hole diameters downstream of the injection holes (x/d=96.6) as a consequence of vortex secondary flows which first sweep injectant in the spanwise direction along the wall and then into upwash regions. St/Sto values are generally lower than Stf/Sto beneath vortex upwash regions since extra injectant accumulates resulting in local increases of protection by the film. In contrast, vortex disruptions are quite small just downstream of the injection holes at x/d=6.7, which indicates that the film, rather than the vortices, is most affecting local heat transfer behavior at this streamwise location.

ACKNOWLEDGEMENTS

This study was supported, in part, by the Aero-Propulsion Laboratory of Wright Patterson Air Force Base, MIPR Number FY 1455-89-N0670. Dr. Bill Troha was program monitor. Some of the facilities used were purchased using funds from the Naval

Postgraduate School Foundation Research Program.

REFERENCES

Bishop D. T., 1990, "Heat Transfer, Adiabatic Effectiveness and Injectant Distributions Downstream of Single and Double Rows of Film-Cooling Holes with Compound Angles," M. S. Thesis, Department of Mechanical Engineering, Naval Postgraduate School, Monterey, Ca.

Blair M. F., 1974, "An Experimental Study of Heat Transfer and Film Cooling on Large-Scale Turbine Endwalls," ASME Transactions-Journal of Heat Transfer, Vol. 96, pp. 524-529.

Eibeck P. A., and Eaton J. K., 1987, "Heat Transfer Effects of a Longitudinal Vortex Embedded in a Turbulent Boundary Layer," ASME Transactions-Journal of Heat Transfer, Vol. 109, pp.16-24.

Folayan C. O., and Whitelaw J. H., 1976, "The Effectiveness of Two-Dimensional Film-Cooling Over Curved Surfaces, " ASME Paper No. 76-HT-31.

Goldstein R. J. and Chen H. P., 1985, "Film Cooling on a Gas Turbine Blade Near the Endwall," ASME Transactions-Journal of Engineering for Gas Turbines and Power, Vol. 107, pp. 117-122.

Goldstein R. J. and Chen H. P., 1987, "Film Cooling of a Turbine Blade with Injection Through Two Rows of Holes in the Near-Endwall Region," American Society of Mechanical Engineers Paper No. 87-GT-196, pp. 1-7.

Kays W.M. and Crawford M. E., 1980, Convective Heat and Mass Transfer, Second Edition, McGraw-Hill Book Company, New York.

Kline S. J. and McClintock F. A., 1953, "Describing Uncertainties in Single-Sample Experiments," Mechanical Engineeering.

Ligrani P. M., Ortiz A., Joseph S. L., and Evans D. L., 1989a, "Effects of Embedded Vortices on Film-Cooled Turbulent Boundary Layers," ASME Transactions-Journal of Turbomachinery, Vol. 111, No. 1, pp. 71-77.

Ligrani P. M., Singer B. A. and Baun L. R., 1989b, "Spatial Resolution and Downwash Velocity Corrections for Multiple-Hole Pressure Probes in Complex Flows," Experiments in Fluids, Vol. 7, No. 6, pp. 424-426.

Ligrani P. M., Singer B. A. and Baun L. R., 1989c, "Miniature Five-Hole Pressure Probe for Measurement of Mean Velocity Components in Low Speed Flows, " Journal of Physics E-Scientific Instruments, Vol. 22, No. 10, pp. 868-876.

Ligrani P. M., and Williams W. W., 1990, "Effects of an Embedded Vortex on Injectant From a Single Film-Cooling Hole in a Turbulent Boundary Layer," ASME Transactions-Journal of Turbomachinery, Vol. 112, No. 3, pp. 428-436.

Ligrani P. M., Subramanian C. S., Craig D. W., and Kaisuwan P., 1991, "Effects of Vortices With Different Circulations on Heat Transfer and Injectant Downstream of a Row of Film-Cooling Holes in a Turbulent Boundary Layer," ASME Transactions-Journal of Heat Transfer, Vol. 113, No. 1, pp. 79-90.

Mayle R. E., Kopper F. C., Blair M. F., and Bailey D. A., 1977, "Effect of Streamline Curvature of Film Cooling, " ASME Transactions-Journal of Engineering for Power, Vol. 99, No. 1, pp.77-82.

Moffat R. J., 1982, "Contributions to the Theory of Single-Sample Uncertainty Analysis," ASME Transactions-Journal of Fluids Engineering, Vol. 104, pp.250-260.

Nicolas J., and Le Meur A., 1974, "Curvature Effects on a Turbine Blade Cooling Film," ASME Paper NO. 74-GT-156.

Ortiz A., 1987, "The Thermal Behavior of Film Cooled Turbulent Boundary Layers as Affected by Longitudinal Vortices," M. S. Thesis, Department of Mechanical Engineering, Naval Postgraduate School, Monterey, Ca.